NPS-MAE-23-006

NAVAL POSTGRADUATE SCHOOL

MONTEREY, CALIFORNIA

TECHNICAL REPORT

TIME-CRITICAL COOPERATIVE PATH FOLLOWING FOR CLANDESTINE MINE COUNTERMEASURES

by

Isaac Kaminer
Sean Kragelund

October 2023

Prepared for: Mine Countermeasure Technical Division, Surface and Mine Warfighting Development Center. This research is supported by funding from the Naval Postgraduate School, Naval Research Program (PE 0605853N/2098). NRP Project ID: NPS-23-N074

THIS PAGE INTENTIONALLY LEFT BLANK

REPORT DOCUMENTATION PAGE

1. REPORT DATE	2. REPORT TYPE	3. DATES COVERED	
		START DATE	END DATE
10/21/2023	Technical report	10/23/2022	10/21/2023

4. TITLE AND SUBTITLE

Time-critical Cooperative Path Following for Clandestine Mine Countermeasures

5a. CONTRACT NUMBER	5b. GRANT NUMBER	5c. PROGRAM ELEMENT NUMBER
		0605853N/2098
5d. PROJECT NUMBER	**5e. TASK NUMBER**	**5f. WORK UNIT NUMBER**
NPS-23-N074-A; W2324		

6. AUTHOR(S)

Isaac Kaminer, Sean Kragelund

7. PERFORMING ORGANIZATION NAME(S) AND ADDRESS(ES)

Naval Postgraduate School
1 University Circle
Monterey, CA 93943-5000

8. PERFORMING ORGANIZATION REPORT NUMBER

NPS-MAE-23-006

9. SPONSORING/MONITORING AGENCY NAME(S) AND ADDRESS(ES)	10. SPONSOR/MONITOR'S ACRONYM(S)	11. SPONSOR/MONITOR'S REPORT NUMBER(S)
Naval Postgraduate School, Naval Research Program; Mine Countermeasure Technical Division, Surface and Mine Warfighting Development	NRP; MCMTD, SMWDC	NPS-23-N074-A

12. DISTRIBUTION/AVAILABILITY STATEMENT

Approved for public release. Distribution is unlimited.

13. SUPPLEMENTARY NOTES

The views expressed in this document are those of the author and do not reflect the official policy or position of the Department of Defense or the U.S. Government.

14. ABSTRACT

15. SUBJECT TERMS

cooperative path planning, autonomous underwater vehicles, mine countermeasures, MCM, AUV

16. SECURITY CLASSIFICATION OF:			17. LIMITATION OF ABSTRACT	18. NUMBER OF PAGES
a. REPORT	b. ABSTRACT	C. THIS PAGE		
U	U	U	UU	32

19a. NAME OF RESPONSIBLE PERSON	19b. PHONE NUMBER *(Include area code)*
Sean Kragelund	(831) 656-1159

THIS PAGE INTENTIONALLY LEFT BLANK

NAVAL POSTGRADUATE SCHOOL
Monterey, California 93943-5000

Ann E. Rondeau
President

Scott Gartner
Provost

The report entitled "Time-critical Cooperative Path Following for Clandestine Mine Countermeasures" was prepared for Mine Countermeasure Technical Division, Surface and Mine Warfighting Development Center and funded by the Naval Postgraduate School, Naval Research Program (PE 0605853N/2098).

Further distribution of all or part of this report is authorized.

This report was prepared by:

Isaac Kaminer
Digitally signed by Isaac Kaminer
Date: 2023.11.09 15:16:32 -08'00'

Isaac Kaminer
Professor

KRAGELUND.SEAN.P.1259139895
Digitally signed by KRAGELUND.SEAN.P.1259139895
Date: 2023.11.09 12:15:52 -08'00'

Sean Kragelund
Research Assistant Professor

Reviewed by:

BINGHAM.BRIAN.STEVEN.1504993910
Digitally signed by BINGHAM.BRIAN.STEVEN.1504993910
Date: 2023.11.09 15:27:15 -08'00'

Brian Bingham, Chairman
Mechanical and Aerospace Engineering

Released by:

SMITH.KEVIN.B.1230026366
Digitally signed by SMITH.KEVIN.B.1230026366
Date: 2023.11.13 14:55:40 -08'00'

Kevin B. Smith
Vice Provost for Research

THIS PAGE INTENTIONALLY LEFT BLANK

List of Acronyms and Abbreviations

AUV	autonomous underwater vehicle
CPF	cooperative path following
ETC	event-triggered communications
GNSS	global navigation satellite system
GUES	globally uniformly exponentially stable
MCM	mine countermeasures
RF	radio frequency
TCCPF	time-critical cooperative path following
QoS	quality of service

THIS PAGE INTENTIONALLY LEFT BLANK

1 Introduction

In contested areas, where Naval forces may not be able to establish a permissive environment for airborne or surface mine countermeasures (MCM), autonomous underwater vehicle (AUV) teams can still conduct underwater MCM missions. In order for these systems to operate clandestinely, without breaching the surface to obtain global navigation satellite system (GNSS) fixes or receive radio frequency (RF) transmissions, AUVs must be able to coordinate their actions using only intermittent, range-limited acoustic communications. This need is heightened for time-critical missions.

The goal of this study was to investigate methods for an AUV team to conduct collaborative search in a contested environment where intermittent, range-limited communications are the only available coordination mechanism. A promising approach which has received a great deal of attention in the literature is time-critical cooperative path following (CPF), or TCCPF. Cooperative path following has played a key role in solving challenging problems such as 1) search and rescue missions, where multiple vehicles progress in coordinated fashion to cover a large area in a shorter amount of time; 2) sequential safe auto-landings, where multiple aerial vehicles arrive at a specified glide slope safely separated by a predefined time interval; and 3) oceanographic science missions, where multiple vehicles work cooperatively to collect sample data from a region of interest. The key requirement that the CPF framework was developed to address was guaranteeing the simultaneous arrival of each vehicle at the end of its desired trajectory. The framework includes three steps:

1. Generate a set of collision-free desired trajectories to be assigned to each vehicle which minimize a given objective function, guarantee obstacle avoidance, and satisfy the simultaneous arrival requirement, defined boundary conditions, and vehicle dynamic constraints [1], [2], [3].
2. Design a path-following control law [4] that steers a vehicle along its desired trajectory.
3. Develop a decentralized time-coordination algorithm that enables each vehicle to a) transmit progress along its desired trajectory to its neighbors; and b) adjust its speed of progression based on information from its neighbors. This step guarantees simultaneous time of arrival by all vehicles, even in the presence of disturbances.

Previous work addressing Step 3, e.g., in [5] and [6], assumed that the topology of the underlying communication network is represented by a connected bidirectional graph with a fixed

topology. However, this is a strong assumption less likely to be satisfied by a typical communication network with time-varying network topology. To address this issue, researchers in [7], [8] were able to guarantee convergence of the time-coordination algorithms for the case where the network topology is represented by a time-varying bidirectional graph that is connected in an integral sense. This condition was used in [9] and [10] to show that collision avoidance can be achieved as well as time-coordination.

Our recent work [11] has shown convergence of time-coordination algorithms for a more general connectivity condition, when the communication network is no longer required to be bidirectional. In fact, we have shown that connectedness of the directed graph in an integral sense is sufficient to achieve convergence. We note, however, that all of the algorithms discussed above rely on continuous or piecewise continuous communications, which may be undesirable or unavailable in real-world applications. Typical examples include underwater MCM missions where communication bandwidth is severely limited and stealth is of paramount importance.

This issue can be overcome by resorting to event-triggered communications (ETC) and control algorithms. With this approach, the communication and control input updates occur only when a predefined condition is satisfied, thereby significantly reducing inter-vehicle communications needed to achieve consensus on the variables of interest. It was pioneered by [12], [13]. Most of the current work in this area assumes that the network topology is either a static bidirectional graph [12]–[15] or digraph [16], [17]. Recently, some algorithms have been proposed which assume the network is a time-varying bidirectional graph [18]–[20] or digraph [21]–[23].

The TCCPF framework has potential for both terrain-relative underwater navigation and multi-vehicle coordination. For example, AUV navigation errors increase with distance from known landmarks, but decrease as AUVs approach them. To bound accumulated localization errors, therefore, path planning must incorporate periodic excursions that revisit these landmarks. Likewise, communications limitations require that AUVs must cooperatively plan to rendezvous at suitable locations for information exchange. Existing ETC algorithms, however, must be modified to explicitly address time-coordination via intermittent, range-limited communications. This report describes a novel ETC algorithm to achieve TCCPF for clandestine MCM. To represent the limitations of acoustic commu-

nications, the underlying network is assumed to be a time-varying digraph connected in an integral sense. Moreover, each AUV transmits its progression information only when a decentralized trigger condition is satisfied, thereby significantly reducing inter-vehicle communication requirements, particularly compared to previous time-coordination algorithms based on continuous communications, e.g., in [5]–[8].

The rest of this report is organized as follows. Section 2 provides a brief review of graph theory. Section 3 formulates the time-coordination problem and presents assumptions on the inter-vehicle information flow. In Section 4, the time-coordination control law based on event-triggered communication is described, and the performance of the time-coordination algorithm is analyzed in the main theorem. In Section 5, simulation results validate the efficacy of the proposed algorithm. Finally, Section 6 presents some conclusions.

2 Preliminaries

2.1 Graph Theory

Adopting the notation of [11], a brief review of graph theory follows. A digraph of size n is defined by $\mathcal{D} = (\mathcal{V}, \mathcal{E}, \mathcal{A})$, where $\mathcal{V} = \{1, \ldots, n\}$ is the set of nodes, $\mathcal{E}$ is the set of edges, and $\mathcal{A}$ is the Adjacency matrix. An edge is denoted by an ordered pair (i, j), which means information can be transmitted from node j to node i. The Adjacency matrix $\mathcal{A}$ is constructed as follows: if $(i, j) \in \mathcal{E}$, one has $\mathcal{A}_{ij} = 1$. Otherwise, $\mathcal{A}_{ij} = 0$. The digraph $\mathcal{D}$ is represented by the Laplacian $L \triangleq \Delta - \mathcal{A}$, where Δ is a diagonal matrix with $\Delta_{ii} \triangleq \sum_{j=1, j\neq i}^{n} \mathcal{A}_{ij}$. The neighborhood of node i is the set $\mathcal{N}_i \triangleq \{j \in \mathcal{V} : (i, j) \in \mathcal{E}\}$. A directed path from node i_s to node i_0 is a sequence of edges (i_0, i_1), (i_1, i_2), $\ldots$, (i_{s-1}, i_s). The digraph $\mathcal{D}$ contains a directed spanning tree if there exists a node such that it can reach every other node via a directed path.

Given a time-varying digraph $\mathcal{D}(t)$, we consider the digraph represented by the integrated Laplacian $\int_t^{t+T} L(\tau)d\tau$. An edge (i, j) in it is said to be a δ-edge if $\int_t^{t+T} -L_{ij}(\tau)d\tau \geq \delta$. A path in it is said to be a δ-path if every edge on the path is a δ-edge.

3 Time-coordinated Path-Following Framework

3.1 Path Following for a Single AUV

A trajectory generation algorithm such as [1], [2] produces a set of collision-free desired trajectories for n AUVs

$$p_{d,i}(t_f) : [0, t_f] \rightarrow \mathbb{R}^3, \;\; i \in \{1, \ldots, n\}, \tag{1}$$

where t_f is the simultaneous time of arrival. Introducing an adjustable non-decreasing function $\gamma_i(t)$ as a coordination state or virtual time

$$\gamma_i(t) : [0, \infty) \rightarrow [0, t_f], \quad i \in \{1, \ldots, n\},$$

we can denote the desired position of the ith AUV as $p_{d,i}(\gamma_i(t))$. This simple idea introduces an additional degree of freedom that allows one to adjust the progression speed of the AUV along its trajectory by controlling $\gamma_i(t)$ and thus to guarantee simultaneous arrival at $t = t_f$ in the presence of disturbances. The control law for $\gamma_i(t)$ will be presented in Section 4.

To have the AUV track $p_{d,i}(\gamma_i(t))$, a path-following control law is needed. This can be done by driving the path-following error

$$e_{PF,i}(t) \triangleq p_i(t) - p_{d,i}(\gamma_i(t)), \quad i \in \{1, \ldots, n\},$$

to zero. In the above expression, $p_i(t)$ represents the actual position of the AUV. In [4], the authors formulated a path-following control law which ensures that the error converges exponentially to zero with ideal performance of the inner-loop autopilot and to a neighborhood of zero with non-ideal one. In other words, in the latter case, there exists $\rho > 0$ such that

$$\|e_{PF}(t)\| \leq \rho, \quad \forall t \geq 0, \tag{2}$$

where $e_{PF}(t) = [e_{PF,1}(t)^\top, \ldots, e_{PF,n}(t)^\top]^\top$.

3.2 Time Coordination for Multiple AUVs

As discussed in the previous subsection, the progression of the AUV along its trajectory can be controlled by adjusting $\gamma_i(t)$. As in [11], we also impose the following objectives.

First, the cooperating AUVs are said to be synchronized at time t, if

$$\gamma_i(t) = \gamma_j(t), \quad \forall i, j \in \{1, \ldots, n\}. \tag{3}$$

Next, for a desired mission completion rate $\dot{\gamma}_d(t) > 0$, if

$$\dot{\gamma}_i(t) = \dot{\gamma}_d(t), \quad \forall i \in \{1, \ldots, n\}, \tag{4}$$

then the AUVs are progressing along their trajectories at the desired mission completion rate.

To satisfy the above requirements, AUVs need to exchange the coordination states $\gamma_i(t)$ with their neighbors over a time-varying directed network. This interaction among the AUVs can be modeled using graph theory (see Section 2).

Finally, the nature of inter-vehicle communications used for our MCM application is based on the assumptions in [11], which are restated below for convenience.

Assumption 1. The information flow between any two AUVs is directional without time delays.

Assumption 2. The ith AUV can receive coordination state $\gamma_j(t)$ only from other AUVs in its neighborhood set $\mathcal{N}_i(t)$, where $j \in \mathcal{N}_i(t)$.

The topology of the underlying communication network $\mathcal{D}(t)$ described by the Laplacian $L(t)$ varies in a way that satisfies the following assumption.

Assumption 3. For all $t \geq 0$, there exists $T > 0$ such that the digraph represented by $\int_t^{t+T} L(\tau)d\tau$ contains a δ-spanning tree. That is, a root node in it can reach every other node via a δ-path.

Remark 1. The network quality of service (QoS) is determined by the parameters $T > 0$ and $\delta \in (0, T]$. With a smaller value of T and a value of δ closer to T, the information flow has stronger connectivity.

Remark 2. Notice that Assumption 3 requires only connectedness in an integral sense, not pointwise in time. Thus, even if the network is disconnected for a certain period of time or at all times, this assumption can still be satisfied.

Problem (Time-Coordinated Path-Following Problem): Given a set of desired trajectories (1) and a path-following control law that ensures (2), design a decentralized time-coordination control law such that the coordination states $\gamma_i(t)$ converge for all i exponentially near the equilibrium (3) and (4) under Assumptions 1, 2, and 3.

Remark 3. Designing a time-coordination control law for the coordination states $\gamma_i(t)$ that solves the Time-Coordinated Path-Following Problem guarantees the simultaneous arrival of all the AUVs at their respective destinations.

4 Main Result

In this section, a decentralized time-coordination algorithm based on ETC is presented.

We propose the following decentralized control law:

$$\begin{aligned}\ddot{\gamma}_i(t) &= -b(\dot{\gamma}_i(t) - \dot{\gamma}_d(t)) \\ &\quad -a \sum_{j \in \mathcal{N}_i(t)} (\gamma_i(t) - \hat{\gamma}_j(t)) + \bar{\alpha}_i(e_{PF,i}(t)), \\ \gamma_i(0) &= \gamma_{i0}, \;\; \dot{\gamma}_i(0) = \dot{\gamma}_{i0},\end{aligned} \tag{5}$$

where a and b are positive coordination control gains and $\bar{\alpha}_i(e_{PF,i}(t))$ is defined as

$$\bar{\alpha}_i(e_{PF,i}(t)) = \frac{\dot{p}_{d,i}(\gamma_i(t))^\top e_{PF,i}(t)}{\|\dot{p}_{d,i}(\gamma_i(t))\| + \eta} \tag{6}$$

with η being a positive design parameter.

Remark 4. The term $\bar{\alpha}_i(e_{PF,i}(t))$ is designed in a way that helps the AUV remain inside the region of attraction of the path-following controller [4]. When it precedes (falls behind of) the desired place, the numerator becomes positive (negative), which accelerates (decelerates) progression of the desired position along the trajectory leading to reduction in $\|e_{PF,i}(t)\|$.

In (5), an estimate $\hat{\gamma}_j(t)$ of $\gamma_j(t)$ is used because the ith AUV intermittently receives $\gamma_j(t)$

from the jth AUV employing ETC. Therefore, it is a reasonable strategy for the ith AUV to estimate $\hat{\gamma}_j(t)$ and to use this estimate to adjust its coordination state $\gamma_i(t)$. The estimator of $\gamma_j(t)$ is given below:

$$\hat{\gamma}_j(t): \begin{cases} \ddot{\hat{\gamma}}_j(t) = -b(\dot{\hat{\gamma}}_j(t) - \dot{\gamma}_d(t)), \ \ t \geq t^j_{k_j(t)} \\ \dot{\hat{\gamma}}_j(t^j_{k_j(t)}) = \dot{\gamma}_j(t^j_{k_j(t)}), \ \ \hat{\gamma}_j(t^j_{k_j(t)}) = \gamma_j(t^j_{k_j(t)}) \end{cases}, \tag{7}$$

where $t^j_{k_j(t)}$ denotes the most recent time the jth AUV transmitted its coordination state $\gamma_j(t)$.

Let the estimation error be $e_j(t) \triangleq \hat{\gamma}_j(t) - \gamma_j(t)$. Then (5) can be rewritten as follows:

$$\begin{aligned} \ddot{\gamma}_i(t) = &-b(\dot{\gamma}_i(t) - \dot{\gamma}_d(t)) - a \sum_{j \in \mathcal{N}_i(t)} (\gamma_i(t) - \gamma_j(t)) \\ &+a \sum_{j \in \mathcal{N}_i(t)} e_j(t) + \bar{\alpha}_i(e_{PF,i}(t)), \\ \gamma_i(0) = \gamma_{i0}, \ \ &\dot{\gamma}_i(0) = \dot{\gamma}_{i0}. \end{aligned} \tag{8}$$

As it can be seen in (8), the error $e_j(t)$ has an explicit impact on the time-coordination dynamics. The key point of the ETC algorithm is to ensure that $|e_j(t)|$ remains bounded. Therefore, when $|e_j(t)|$ reaches a given threshold, i.e., a transmission event is triggered, the jth AUV transmits the time instant t at which this event occurred as well as $\gamma_j(t)$, $\dot{\gamma}_j(t)$. To be more specific, we define an event-triggering function $\delta_j(t)$ as

$$\delta_j(t) = |e_j(t)| - h(t), \tag{9}$$

where $h(t) = c_1 + c_2 e^{-at}$, $c_1, c_2, a \in \mathbb{R}_{\geq 0}$ is referred to as a threshold function, and $c_1 \leq h(t) \leq c_1 + c_2$. Whenever $\delta_j(t) > 0$, sampling and transmission take place with $|e_j(t)|$ reset to 0. With this ETC algorithm, boundedness of the error is guaranteed: $|e_j(t)| \leq h(t)$.

Remark 5. The ith AUV uses the estimator (7) to propagate the time-coordination controller (5). On the other hand, the jth AUV executes the same code to check whether the event triggering condition $|e_j(t)| > h(t)$ is satisfied.

Remark 6. Due to the time-varying nature of the underlying network, there might be no available transmission channels when sampling occurs. Then the AUV continues sampling

the data irrespective of the network topology and transmits the most recently sampled data $(t^j_{k_j(t)}, \gamma_j(t^j_{k_j(t)}), \dot{\gamma}_j(t^j_{k_j(t)}))$ when it has available transmission channels.

For the ease of stability analysis, we introduce the coordination error state $\xi_{TC}(t) = [\xi_1(t)^\top \ \xi_2(t)^\top]^\top$ with

$$\begin{aligned} \xi_1(t) &= Q\gamma(t) \ \in \mathbb{R}^{n-1}, \\ \xi_2(t) &= \dot{\gamma}(t) - \dot{\gamma}_d(t)1_n \ \in \mathbb{R}^n, \end{aligned} \tag{10}$$

where $\gamma(t) = [\gamma_1(t), \ldots, \gamma_n(t)]^\top$, and $Q \in \mathbb{R}^{(n-1)\times n}$ is a matrix that satisfies $Q1_n = 0_{n-1}$ and $QQ^\top = \mathbb{I}_{n-1}$.

Remark 7. A matrix $Q_k \in \mathbb{R}^{(k-1)\times k}$, $k \geq 2$, satisfying $Q_k 1_k = 0_{k-1}$ and $Q_k \ (Q_k)^\top = \mathbb{I}_{k-1}$, can be constructed recursively:

$$Q_k = \begin{bmatrix} \sqrt{\frac{k-1}{k}} & -\frac{1}{\sqrt{k(k-1)}} 1^\top_{k-1} \\ 0 & Q_{k-1} \end{bmatrix}$$

with initial condition $Q_2 = [1/\sqrt{2} \ -1/\sqrt{2}]$. For notational simplicity, we denote Q_n by Q, where n is the number of the AUVs.

It is shown in [24, Lemma 7] that $Q^\top Q = \mathbb{I}_n - \frac{1_n 1_n^\top}{n}$ and the nullspace of Q is spanned by 1_n. Now suppose that $\xi_1(t) = Q\gamma(t) = 0_{n-1}$. Then since the nullspace of Q is spanned by 1_n, we obtain that $\gamma_i(t) = \gamma_j(t)$, $\forall i, j \in \{1, \ldots, n\}$. Furthermore, $\xi_2(t) = 0_n$ implies that $\dot{\gamma}_i(t) = \dot{\gamma}_d(t)$, $\forall i \in \{1, \ldots, n\}$. Therefore, $\xi_{TC}(t) = 0_{2n-1}$ is equivalent to (3) and (4).

Using definitions of $\gamma(t)$, $L(t)$ and $\mathcal{A}(t)$, the expression (8) can be rewritten in a more compact form

$$\begin{aligned} \ddot{\gamma}(t) &= -b\xi_2(t) - aL(t)\gamma(t) + a\mathcal{A}(t)e(t) + \bar{\alpha}(e_{PF}(t)), \\ \gamma(0) &= \gamma_0, \ \ \dot{\gamma}(0) = \dot{\gamma}_0, \end{aligned}$$

where $\bar{\alpha}(e_{PF} \ (t)) = [\bar{\alpha}_1(e_{PF,1}(t)), \ldots, \bar{\alpha}_n(e_{PF,n}(t))]^\top$ and $e(t) = [e_1(t), \ldots, e_n(t)]^\top$.

Lemma 1. *Consider the following dynamics:*

$$\dot{x} = -\frac{a}{b} L(t)x, \quad x(0) = x_0 \in \mathbb{R}^n. \tag{11}$$

Under Assumption 3 on $L(t)$, the components x_i's of x reach consensus exponentially

$$diam\,(x\,(t)) \triangleq \max_i\{x_i(t)\} - \min_i\{x_i(t)\} \tag{12}$$

$$\leq diam\,(x(0))\,k e^{-\lambda t}, \tag{13}$$

where $k \triangleq \frac{1}{1-(\delta')^n}$ *and* $\lambda \triangleq -\frac{1}{nT}\ln(1-(\delta')^n)$ *with* $\delta' \triangleq \min\left\{1, \frac{a}{b}\delta\right\} e^{-(n-1)\frac{a}{b}T}$.

Proof. The proof follows from the first half of the proof of [22, Theorem 1]. □

Lemma 2. *The quantities* $\|Qx\|$ *and* $diam(x)$ *satisfy the following inequalities:*

$$\frac{1}{\sqrt{n}}\|Qx\| \leq diam(x) \leq \sqrt{2}\|Qx\|. \tag{14}$$

Proof. The first inequality in (14) follows from

$$\|Qx\|^2 = x^\top Q^\top Qx = x^\top\left(\mathbb{I}_n - \frac{1_n 1_n^\top}{n}\right)x = n\left\{\frac{1}{n}\sum_{i=1}^n x_i^2 - \left(\frac{1_n^\top x}{n}\right)^2\right\}$$

$$= \sum_{i=1}^n\left(x_i - \frac{1_n^\top x}{n}\right)^2 \leq n\left(\max_i\{x_i\} - \min_i\{x_i\}\right)^2 = n\,\{diam(x)\}^2$$

The second inequality in (14) follows from

$$\{diam(x)\}^2 = \left(\max_i\{x_i\} - \min_i\{x_i\}\right)^2 = \left(\max_i\{x_i\} - \frac{1_n^\top x}{n} + \frac{1_n^\top x}{n} - \min_i\{x_i\}\right)^2$$

$$\leq 2\left(\max_i\{x_i\} - \frac{1_n^\top x}{n}\right)^2 + 2\left(\frac{1_n^\top x}{n} - \min_i\{x_i\}\right)^2 \leq 2\sum_{i=1}^n\left(x_i - \frac{1_n^\top x}{n}\right)^2 = 2\|Qx\|^2$$

□

Remark 8. When the elements x_i of a vector x reach consensus, i.e., $x_1 = \cdots = x_n$, both $\|Qx\|$ and $diam(x)$ are zero. Otherwise, they have positive values, which become larger as x_i's diverge away from consensus. In other words, $\|Qx\|$ and $diam(x)$ quantify the discoordination among x_i's. Moreover, Lemma 2 implies that $\|Qx\|$ and $diam(x)$ are equivalent measures of the discoordination among x_i's.

The main results of the paper are presented in the following theorem.

Theorem 1. *Consider a set of desired trajectories* (1) *and a path-following controller that ensures* (2)*. Let the evolution of $\gamma_i(t)$ be governed by* (5) *over the network $\mathcal{D}(t)$ satisfying Assumption 3. Then, there exist time coordination control gains a, b, and η such that*

$$\begin{aligned}\|\xi_{TC}(t)\| \leq \kappa_1 \|\xi_{TC}(0)\| e^{-\lambda_{TC} t} \\ +\kappa_2 \sup_{t\geq 0} \left(an\sqrt{n}h(t) + \|e_{PF}(t)\| + |\ddot{\gamma}_d(t)|\right)\end{aligned}$$

with rate of convergence

$$\lambda_{TC} \leq \frac{\lambda}{6nk^2}, \tag{15}$$

where λ and k were defined in Lemma 1.

Moreover, the event-triggered time interval $t^i_{k+1} - t^i_k$ is bounded below. Here, t^i_k denotes the kth event-triggered time of the ith AUV.

Proof. Motivated by [8], we introduce a new state

$$\chi(t) = b\xi_1(t) + Q\xi_2(t).$$

Then, the coordination error state $\xi_{TC}(t) = [\xi_1(t)^\top \ \xi_2(t)^\top]^\top$ can be redefined as $\bar{\xi}_{TC}(t) = [\chi(t)^\top \ \xi_2(t)^\top]^\top$ with dynamics

$$\begin{aligned}\dot{\chi} &= -\frac{a}{b}\bar{L}(t)\chi + \frac{a}{b}QL(t)\xi_2 + aQ\mathcal{A}(t)e + Q\bar{\alpha}(e_{PF}) \\ \dot{\xi}_2 &= -\frac{a}{b}L(t)Q^\top\chi - \left(b\mathbb{I}_n - \frac{a}{b}L(t)\right)\xi_2 + a\mathcal{A}(t)e \\ &\quad + \bar{\alpha}(e_{PF}) - \ddot{\gamma}_d 1_n,\end{aligned} \tag{16}$$

where $\bar{L}(t) \triangleq QL(t)Q^\top \in \mathbb{R}^{(n-1)\times(n-1)}$.
In order to construct a Lyapunov function candidate for (16), we first show that the following auxiliary system

$$\dot{\phi}(t) = -\frac{a}{b}\bar{L}(t)\phi(t), \quad \phi(0) = \phi_0 \in \mathbb{R}^{n-1} \tag{17}$$

is globally uniformly exponentially stable (GUES). As $Q \in \mathbb{R}^{(n-1)\times n}$ is a full rank matrix, there exists $x_0 \in \mathbb{R}^n$ such that $\phi_0 = Qx_0$. Let $x(t)$ be the solution of (11). Then $Qx(t)$ is a unique solution of (17):

$$\begin{aligned}\dot{\phi} + \frac{a}{b}\bar{L}(t)\phi = Q\dot{x} + \frac{a}{b}\bar{L}(t)Qx &= Q\left(\dot{x} + \frac{a}{b}L(t)Q^\top Qx\right)\\ &= Q\left(\dot{x} + \frac{a}{b}L(t)x\right) \equiv 0,\end{aligned}$$

where the third equality follows from the fact that $L(t)Q^\top Q = L(t)$. Therefore, we have

$$\begin{aligned}\|\phi\| = \|Qx\| &\leq \sqrt{n}\; diam(x) \leq \sqrt{n}\; diam(x_0)ke^{-\lambda t}\\ &\leq \sqrt{n}\big(\sqrt{2}\|Qx_0\|\big)ke^{-\lambda t} = k_\phi\|\phi_0\|e^{-\lambda t},\end{aligned}$$

where $k_\phi \triangleq \sqrt{2n}k$, the second inequality follows from (13), and the other inequalities follow from (14). The GUES of (17) can now be used to define a Lyapunov function candidate to analyze stability of (16) as presented in the subsequent discussion.
Since the system (17) is GUES, Theorem 4.12 in [25] implies that there exists a continuously differentiable, symmetric, positive definite matrix $\Psi(t)$ such that

$$c_1\mathbb{I}_{n-1} \triangleq \frac{bc_3}{2an}\mathbb{I}_{n-1} \leq \Psi(t) \leq \frac{k_\phi^2 c_4}{2\lambda}\mathbb{I}_{n-1} \triangleq c_2\mathbb{I}_{n-1}, \tag{18}$$

$$\dot{\Psi}(t) - \frac{a}{b}\bar{L}^\top(t)\Psi(t) - \frac{a}{b}\Psi(t)\bar{L}(t) \leq -c_3\mathbb{I}_{n-1}, \tag{19}$$

where c_3 and c_4 are any constants satisfying $0 < c_3 \leq c_4$.
Using $\Psi(t)$, we define a Lyapunov function candidate for (16) as follows:

$$V_{TC}(t) = \chi^\top\Psi(t)\chi + \frac{\beta}{2}\|\xi_2\|^2 = \bar{\xi}_{TC}^\top W(t)\bar{\xi}_{TC}, \tag{20}$$

where $\beta > 0$ and $W(t) \triangleq \begin{bmatrix}\Psi(t) & 0\\ 0 & \frac{\beta}{2}\mathbb{I}_n\end{bmatrix}$. Notice that $V_{TC}(t)$ satisfies $z^\top M_1 z \leq V_{TC}(t) \leq z^\top M_2 z$, where $z \triangleq [\|\chi\|\ \|\xi_2\|]^\top$ with

$$M_1 \triangleq \begin{bmatrix}c_1 & 0\\ 0 & \beta/2\end{bmatrix} \text{ and } M_2 \triangleq \begin{bmatrix}c_2 & 0\\ 0 & \beta/2\end{bmatrix}.$$

The time derivative of (20) along the trajectory of (16) satisfies

$$\begin{aligned}\dot{V}_{TC} = &\chi^\top \left(\dot{\Psi}(t) - \frac{a}{b}\bar{L}^\top(t)\Psi(t) - \frac{a}{b}\Psi(t)\bar{L}(t)\right)\chi \\ &-\beta\xi_2^\top \left(b\mathbb{I}_n - \frac{a}{b}L(t)\right)\xi_2 \\ &+\chi^\top \left(2\frac{a}{b}\Psi(t)QL(t) - \beta\frac{a}{b}QL^\top(t)\right)\xi_2 \\ &+ \left(2\chi^\top\Psi(t)Q + \beta\xi_2^\top\right)\left(a\mathcal{A}(t)e + \bar{\alpha}(e_{PF})\right) - \beta\xi_2^\top\ddot{\gamma}_d 1_n,\end{aligned}$$

which leads to

$$\begin{aligned}\dot{V}_{TC} \leq &- c_3\|\chi\|^2 - \beta\left(b - \frac{a}{b}n\right)\|\xi_2\|^2 \\ &+ \left(2\frac{a}{b}n\|\Psi(t)\| + \beta\frac{a}{b}n\right)\|\chi\|\|\xi_2\| \\ &+ \left(2\|\Psi(t)\|\|\chi\| + \beta\|\xi_2\|\right)\left(an\|e\| + \|\bar{\alpha}(e_{PF})\| + |\ddot{\gamma}_d|\right),\end{aligned}$$

where we used (19), $\|Q\| = 1$, $\|L(t)\| \leq n$, and $\|\mathcal{A}(t)\| \leq n$.
Applying $\|\Psi(t)\| \leq c_2 = \frac{k_\phi^2 c_4}{2\lambda}$ in (18) yields

$$\begin{aligned}\dot{V}_{TC} \leq &- c_3\|\chi\|^2 - \beta\left(b - \frac{a}{b}n\right)\|\xi_2\|^2 \\ &+ \left(\frac{a}{b}\frac{nk_\phi^2}{\lambda}c_4 + \beta\frac{a}{b}n\right)\|\chi\|\|\xi_2\| \\ &+ \left(\frac{k_\phi^2 c_4}{\lambda} + \beta\right)\|\bar{\xi}_{TC}\|\left(an\|e\| + \frac{v_{max}}{v_{min} + \eta}\|e_{PF}\| + |\ddot{\gamma}_d|\right),\end{aligned}$$

where $v_{max} = \max_i\{v_{i,max}\}$ and $v_{min} = \max_i\{v_{i,min}\}$ with $v_{i,max}$ and $v_{i,min}$ being the maximum and minimum achievable speed of the ith AUV. Letting $c_3 = c_4$ and $\eta > v_{max} - v_{min}$, one obtains

$$\dot{V}_{TC} \leq -z^\top Uz + \left(\frac{k_\phi^2 c_4}{\lambda} + \beta\right)\|\bar{\xi}_{TC}\|\left(an\|e\| + \|e_{PF}\| + |\ddot{\gamma}_d|\right),$$

where $z = [\|\chi\| \ \|\xi_2\|]^\top$ and

$$U \triangleq \begin{bmatrix} c_3 & -\frac{1}{2}\left(\frac{a}{b}\frac{nk_\phi^2}{\lambda}c_3 + \beta\frac{a}{b}n\right) \\ -\frac{1}{2}\left(\frac{a}{b}\frac{nk_\phi^2}{\lambda}c_3 + \beta\frac{a}{b}n\right) & \beta\left(b - \frac{a}{b}n\right) \end{bmatrix}.$$

Next, we introduce $\lambda_{TC} \leq \frac{2\lambda}{3k_\phi^2} = \frac{\lambda}{6nk^2}$ which defines the time-coordination error convergence rate. Consider

$$\begin{aligned} &U - 3\lambda_{TC}M_2 \\ &= \begin{bmatrix} c_3 - \lambda_{TC}\frac{3k_\phi^2}{2\lambda}c_3 & -\frac{1}{2}\left(\frac{a}{b}\frac{nk_\phi^2}{\lambda}c_3 + \beta\frac{a}{b}n\right) \\ -\frac{1}{2}\left(\frac{a}{b}\frac{nk_\phi^2}{\lambda}c_3 + \beta\frac{a}{b}n\right) & \beta\left(b - \frac{a}{b}n - \frac{3}{2}\lambda_{TC}\right) \end{bmatrix}. \end{aligned} \tag{21}$$

Note that for a fixed value of $\frac{a}{b}$, all the terms in (21) are fixed except for βb in the $(2,2)$ element. This is because the values of k_ϕ and λ are determined by the ratio of $\frac{a}{b}$. Thus, choosing a sufficiently large b with a fixed $\frac{a}{b}$ makes sure that (21) is positive semi-definite. Therefore, we obtain that $-z^\top Uz \leq -3\lambda_{TC}z^\top M_2 z \leq -3\lambda_{TC}V_{TC}$ and thus the derivative of V_{TC} is bounded above by

$$\begin{aligned} \dot{V}_{TC} &\leq -3\lambda_{TC}V_{TC} \\ &\quad + \left(\frac{k_\phi^2 c_3}{\lambda} + \beta\right)\|\bar{\xi}_{TC}\|\left(an\|e\| + \|e_{PF}\| + |\ddot{\gamma}_d|\right) \\ &\leq -2\lambda_{TC}V_{TC} - \lambda_{TC}\min\{c_1, \beta/2\}\|\bar{\xi}_{TC}\|^2 \\ &\quad + \left(\frac{k_\phi^2 c_3}{\lambda} + \beta\right)\|\bar{\xi}_{TC}\|\left(an\|e\| + \|e_{PF}\| + |\ddot{\gamma}_d|\right). \end{aligned}$$

By applying Lemma 4.6 in [25] and introducing the state transformation $\bar{\xi}_{TC} = S\xi_{TC} \triangleq \begin{bmatrix} b\mathbb{I}_{n-1} & Q \\ 0 & \mathbb{I}_n \end{bmatrix}\xi_{TC}$, we conclude that

$$\begin{aligned} \|\xi_{TC}(t)\| \leq \kappa_1\|\xi_{TC}(0)\|e^{-\lambda_{TC}t} \\ +\kappa_2 \sup_{t\geq 0}\left(an\sqrt{n}h(t) + \|e_{PF}(t)\| + |\ddot{\gamma}_d(t)|\right), \end{aligned} \tag{22}$$

where $\|e(t)\| \leq \sqrt{n}h(t)$ was used and

$$\kappa_1 \triangleq \|S^{-1}\|\sqrt{\frac{\max\{c_2, \beta/2\}}{\min\{c1, \beta/2\}}}\|S\|, \tag{23}$$

$$\kappa_2 \triangleq \|S^{-1}\|\sqrt{\frac{\max\{c_2, \beta/2\}}{\min\{c1, \beta/2\}}}\frac{\frac{k_\phi^2 c_3}{\lambda} + \beta}{\lambda_{TC}\min\{c_1, \beta/2\}}. \tag{24}$$

Lastly, we show that $t_{k+1}^i - t_k^i$ is bounded below. From (7) and (8), it follows that the estimation error dynamics can be written in the form of

$$\begin{aligned} \dot{\epsilon}_i(t) &= A\epsilon_i(t) + Bu_i(t), \quad t \in [t_k^i, t_{k+1}^i), \\ \epsilon_i(t_k^i) &= [0\ 0]^\top, \end{aligned} \tag{25}$$

where $\epsilon_i(t) = [e_i(t)\ \dot{e}_i(t)]^\top$, $A = \begin{bmatrix} 0 & 1 \\ 0 & -b \end{bmatrix}$, $B = \begin{bmatrix} 0 \\ 1 \end{bmatrix}$, and $u_i = a\sum_{j\in\mathcal{N}_i}(\gamma_i - \gamma_j) - a\sum_{j\in\mathcal{N}_i} e_j - \bar{\alpha}_i(e_{PF,i})$.

One can show that

$$\begin{aligned} |u_i| &\leq a\|L\gamma\| + a\|\mathcal{A}e\| + \|\bar{\alpha}(e_{PF})\| \\ &\leq a\|L\|\|Q^\top\|\|Q\gamma\| + a\|\mathcal{A}\|\|e\| + \|e_{PF}\| \\ &\leq an\left(\kappa_1\|\xi_{TC}(0)\| + \kappa_2 \sup_{t\geq 0}\left(an\sqrt{n}h(t) + \|e_{PF}\| + |\ddot{\gamma}_d|\right)\right) \\ &\quad + a\|\mathcal{A}\|\|e\| + \|e_{PF}\| \\ &\leq an\kappa_1\|\xi_{TC}(0)\| + an\kappa_2\left(an\sqrt{n}\,(c_1 + c_2) + \rho + \ddot{\gamma}_{d,max}\right) \\ &\quad + an\sqrt{n}(c_1 + c_2) + \rho \triangleq \bar{u}. \end{aligned}$$

Therefore, we can show that the error $e_i(t)$ is bounded above using (25) as follows:

$$\begin{aligned} |e_i| \leq \|\epsilon_i\| &\leq \int_{t_k^i}^{t} (\|A\|\|\epsilon_i\| + \|B\||u_i|)d\tau \\ &\leq \int_{t_k^i}^{t} \|A\|\|\epsilon_i\|d\tau + (t - t_k^i)\|B\|\bar{u}. \end{aligned} \tag{26}$$

Applying the Gronwall-Bellman inequality, see Lemma A.1 in [25], to inequality (26) leads to

$$
\begin{aligned}
|e_i| \leq \|\epsilon_i\| &\leq (t - t_k^i)\|B\|\bar{u} + \|A\| \int_{t_k^i}^{t} (s - t_k^i)\|B\|\bar{u} e^{\|A\|(t-s)} ds \\
&\leq \|B\|\bar{u} \left(e^{\|A\|(t-t_k^i)} - 1 \right) / \|A\|.
\end{aligned}
$$

Considering that the transmission event is triggered when $|e_i(t)| > h(t) \geq c_1$, the inter-event time interval is bounded below:

$$
t_{k+1}^i - t_k^i \geq \frac{1}{\|A\|} \ln \left(1 + c_1 \|A\| / (\|B\|\bar{u}) \right) > 0.
$$

This completes the proof of Theorem 1. □

Remark 9. We note that the rate of convergence λ_{TC} in (15) is determined by $T > 0$ and $\delta \in (0, T]$, which represent the QoS of the underlying network and also by the values of the coordination control gains a and b.

5 Simulation Results

This section presents simulation results of a coordinated path-following mission which illustrates the efficacy of the proposed algorithm. The trajectory generation algorithm described in [2] and [3] first designs a set of Bezier curves with the following specification. From starting points located on the $y = 0\,m$ plane, compute vehicle trajectories which simultaneously reach the $y = 150\,m$ plane after exchanging (x, z) coordinates. The inter-vehicle safety distance is $10\,m$ and the mission duration is $t_f = 21.10\,s$. The solid curves in Figure 1 depict the desired trajectories.

Considering a more general situation, the initial positions of the AUVs are not the same as the initial points of the desired trajectories, i.e., they have initial path-following errors. The path-following controller [4] steers each AUV onto its desired trajectory. The dotted curves in Figure 1 show the paths travelled by the AUVs.

Suppose that the AUVs activate the transmission edges of Figure 2 and that they occur in order $\mathcal{D}_1 \rightarrow \mathcal{D}_2 \rightarrow \mathcal{D}_3 \rightarrow \mathcal{D}_1 \rightarrow \cdots$, each with a duration of $0.03\,s$ due to tight

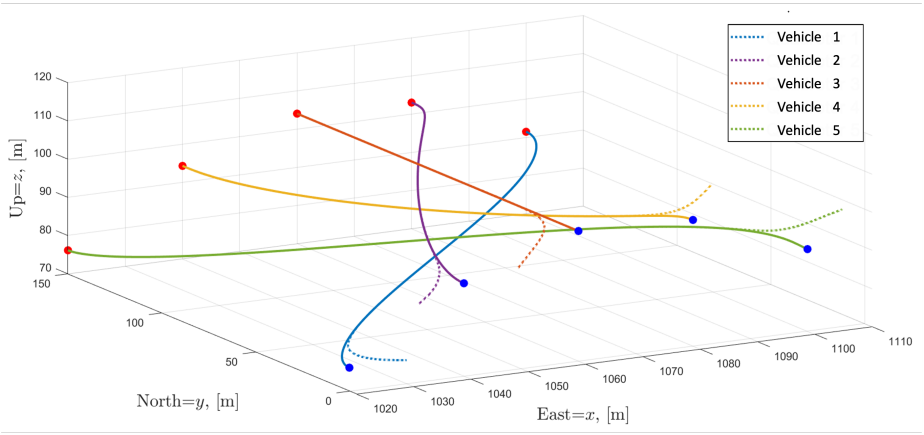

Figure 1. Time-coordinated path-following of five AUVs. The starting points of the desired trajectories, blue dots, are on $y = 0\,m$. The final points, red dots, are on $y = 150\,m$.

communication bandwidth. Even though $\mathcal{D}(t)$ is not connected at all times, the integrated graph represented by $\int_t^{t+0.09} L(\tau)d\tau$ $(\forall t \geq 0)$ contains a 0.03-spanning tree, i.e., it is connected in an integral sense, satisfying the Assumption 3. The coordination control gains and the parameter η in (6) are set to $a = 3.75$, $b = 4.82$, and $\eta = 12$. The initial conditions for the coordination state are $\gamma(0) = 0_n$ and $\dot{\gamma}(0) = 1_n$.

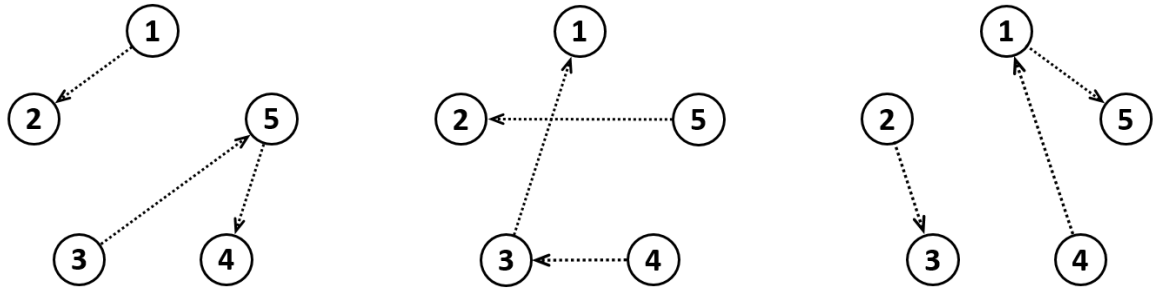

(a) $\mathcal{D}_1$ (b) $\mathcal{D}_2$ (c) $\mathcal{D}_3$

Figure 2. Switching topology of available transmission edges.

Figures 3-6 illustrate how the coordination controller (5) works in combination with (7). Initially, AUVs 1 and 2 start on the $y = 0\,m$ plane, while AUVs 3 and 5 start ahead of it, and AUV 4 starts behind it. By the definition of (6), the term $\bar{\alpha}_i(e_{PF,i}(0))$ is positive for $i = 3, 5$; negative for $i = 4$; and close to zero for the remaining i values. As $\bar{\alpha}_i(e_{PF,i}(t))$ is added to the

right hand side of (5), it makes sense that $\gamma_3(t)$ and $\gamma_5(t)$ accelerate, while $\gamma_4(t)$ decelerates for the first few secondsshown in Figure 3. This evolution of $\gamma_i(t)$ helps each AUV quickly

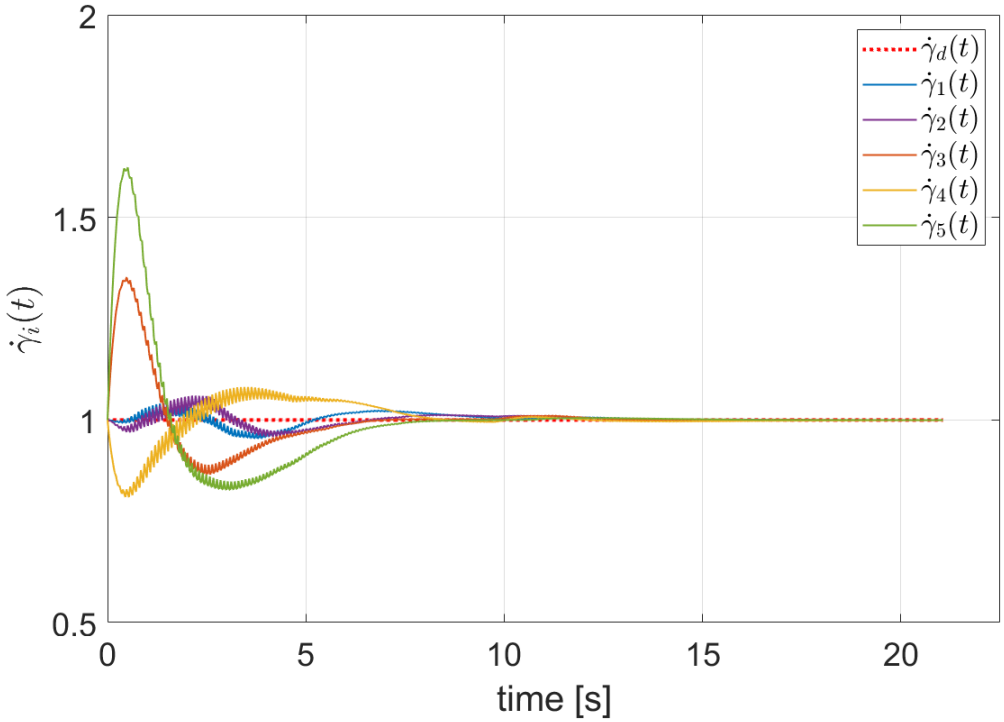

Figure 3. Convergence of $\dot{\gamma}_i(t)$ to a neighborhood of $\dot{\gamma}_d(t) = 1$.

approach its desired position inside the region of attraction as shown in Figure 4. However, this capability comes at the cost of increased inter-vehicle discoordination as illustrated in the first few seconds of Figure 5. This initial discoordination is alleviated by the proposed ETC algorithm. Comparing (5) with (7), we notice that the estimation error $e_i(t) = \hat{\gamma}_i(t) - \gamma_i(t)$ stems from $\bar{\alpha}_i(e_{PF,i}(t))$. With larger values of $\bar{\alpha}_i(e_{PF,i}(0))$ for $i = 3, 4, 5$, the corresponding error $e_i(t)$, $i = 3, 4, 5$ evolves quickly. Sampling and transmission take place whenever the error exceeds the threshold function $h(t) = 0.03$ in our simulation. Figure 6 confirms that AUVs 3, 4, and 5 sample and transmit their data more frequently than the others do. Transmitted data is used by the estimator (7) to update the second term of the controller (5) used to achieve inter-vehicle coordination.

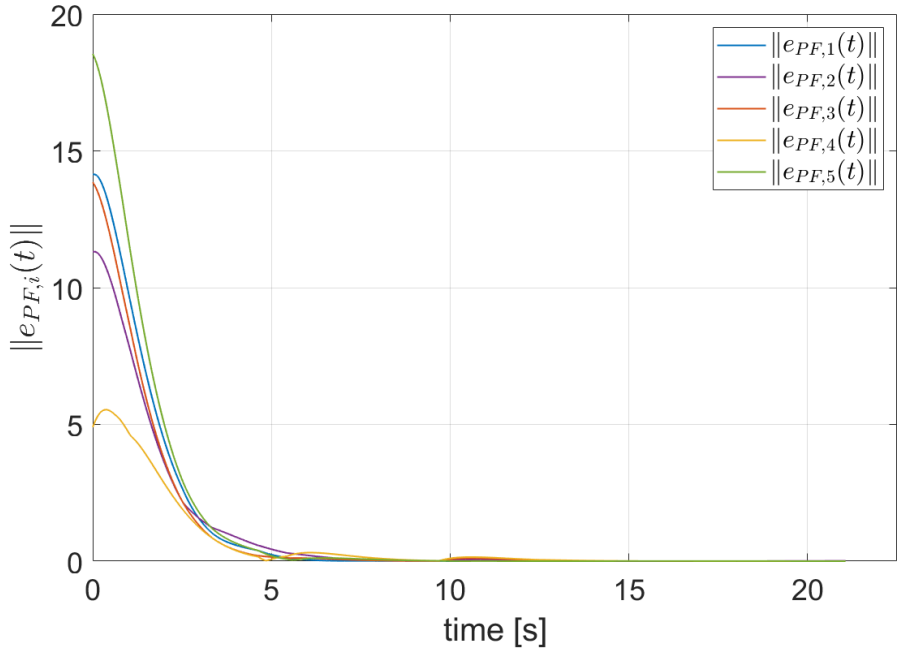

Figure 4. Path-following errors.

In Figures 5 and 6 we observe that once coordination errors become sufficiently small, inter-vehicle communication is triggered less frequently. Using this algorithm, therefore, a team of AUVs will use their limited communications resources more intelligently, i.e., only when needed. If they become discoordinated by disturbances such as wind or currents, they will be able to restore coordination in the same manner.

In simulation, the AUVs simultaneously reach the $y = 150\,m$ plane at $t = 21.06\,s$, which is slightly earlier than the originally scheduled time of $t_f = 21.10\,s$. This occurs because AUVs 3 and 5, initially starting ahead of the $y = 0\,m$ plane, made the mission unfold faster than planned. Of course it is also possible to ensure the AUVs arrive precisely when planned by adjusting $\dot{\gamma}_d(t)$ during their mission from a value of 1 to a smaller value.

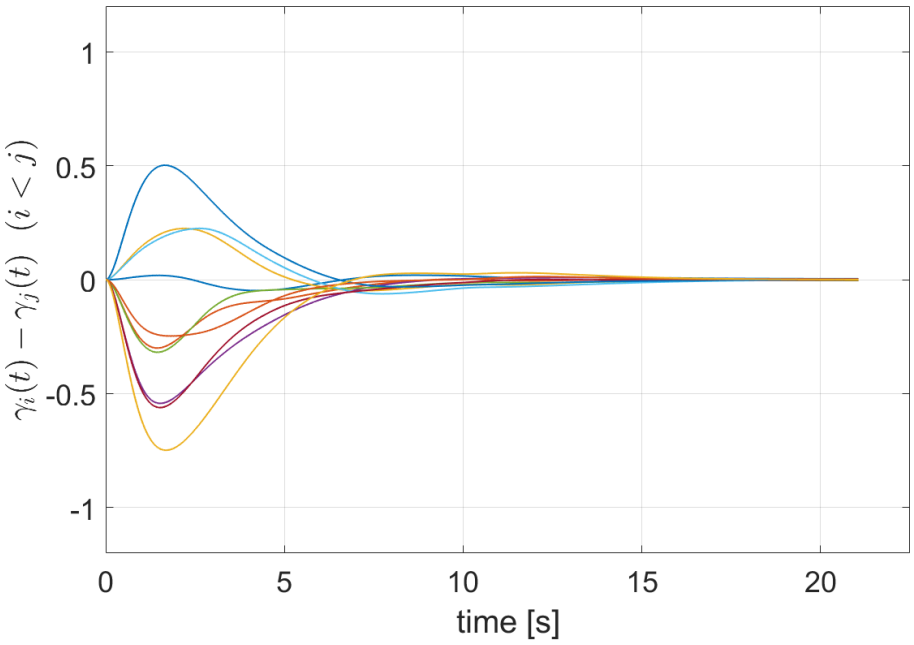

Figure 5. Convergence of the coordination error $\gamma_i(t) - \gamma_j(t)$ $(i < j)$ to a neighborhood of zero.

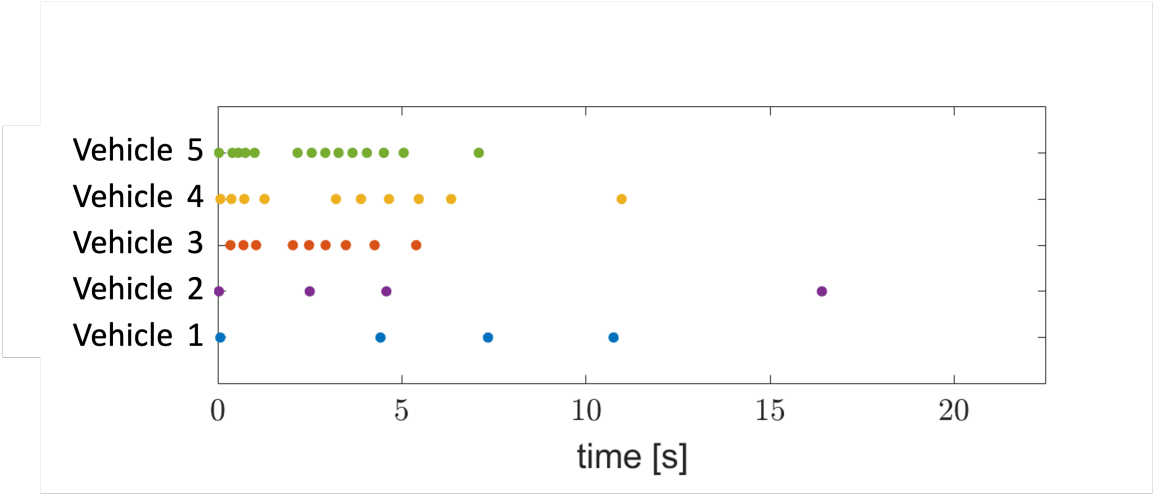

Figure 6. Event-triggered time instances.

6 Conclusion

This report proposed a novel time-coordination algorithm using an event-triggered communication strategy, where the exponential convergence of the coordination errors to a neighborhood of zero was proven. Simulation results validated that coordinating the path following of AUVs is possible using intermittent event-triggered communications. Incorporating this time-coordination algorithm into the existing TCCPF framework has utility for AUV teams conducting underwater MCM missions which must plan trajectories and coordinate their actions via intermittent, range-limited acoustic communications.

References

[1] R. Choe, J. Puig-Navarro, V. Cichella, E. Xargay, and N. Hovakimyan, "Cooperative trajectory generation using pythagorean hodograph bézier curves," *Journal of Guidance, Control, and Dynamics*, vol. 39, no. 8, p. 1744 – 1763, 2016 [Online]. Available: https://doi.org/10.2514/1.G001531

[2] V. Cichella, I. Kaminer, C. Walton, N. Hovakimyan, and A. M. Pascoal, "Optimal multivehicle motion planning using bernstein approximants," *IEEE Transactions on Automatic Control*, vol. 66, no. 4, pp. 1453–1467, 2021 [Online]. Available: https://doi.org/10.1109/TAC.2020.2999329

[3] S. P. Kragelund and I. I. Kaminer, "Clandestine mine countermeasures optimization for autonomy and risk assessment," Naval Postgraduate School, Monterey, California, NPS-MAE-22-004, 2022 [Online]. Available: https://hdl.handle.net/10945/71833

[4] V. Cichella *et al.*, "A 3d path-following approach for a multirotor uav on so(3)," *IFAC Proceedings Volumes*, vol. 46, no. 30, pp. 13–18, 2013. 2nd IFAC Workshop on Research, Education and Development of Unmanned Aerial Systems [Online]. Available: https://doi.org/https://doi.org/10.3182/20131120-3-FR-4045.00039

[5] I. Kaminer, O. Yakimenko, A. Pascoal, and R. Ghabcheloo, "Path generation, path following and coordinated control for timecritical missions of multiple uavs," in *2006 American Control Conference*, 2006, pp. 4906–4913 [Online]. Available: https://doi.org/10.1109/ACC.2006.1657498

[6] R. Ghabcheloo, A. Pascoal, C. Silvestre, and I. Kaminer, "Non-linear co-ordinated path following control of multiple wheeled robots with bidirectional communication constraints," *International Journal of Adaptive Control and Signal Processing*, vol. 21, no. 2-3, p. 133–157, 2007 [Online]. Available: https://doi.org/10.1002/acs.923

[7] E. Xargay *et al.*, "Time-critical cooperative path following of multiple unmanned aerial vehicles over time-varying networks," *Journal of Guidance, Control, and Dynamics*, vol. 36, no. 2, p. 499–516, 2013 [Online]. Available: https://doi.org/10.2514/1.56538

[8] V. Cichella *et al.*, "Cooperative path following of multiple multirotors over time-varying networks," *IEEE Transactions on Automation Science and Engineering*, vol. 12, no. 3, p. 945–957, 2015 [Online]. Available: https://doi.org/10.1109/TASE.2015.2406758

[9] S. B. Mehdi, V. Cichella, T. Marinho, and N. Hovakimyan, "Collision avoidance in multi-vehicle cooperative missions using speed adjustment," in *2017 IEEE 56th Annual Conference on Decision and Control (CDC)*, 2017, pp. 2152–2157 [Online]. Available: https://doi.org/10.1109/CDC.2017.8263963

[10] C. Tabasso, V. Cichella, S. Bilal Mehdi, T. Marinho, and N. Hovakimyan, "Guaranteed collision avoidance in multivehicle cooperative missions using speed adjustment," *Journal of Aerospace Information Systems*, vol. 17, no. 8, p. 436–453, 2020 [Online]. Available: https://doi.org/10.2514/1.i010788

[11] H. Kang, I. Kaminer, V. Cichella, and N. Hovakimyan, "Coordinated path following of quadrotors over time-varying digraphs connected in an integral sense," *arXiv preprint*, 2023.

[12] D. V. Dimarogonas, E. Frazzoli, and K. H. Johansson, "Distributed event-triggered control for multi-agent systems," *IEEE Transactions on Automatic Control*, vol. 57, no. 5, pp. 1291–1297, 2012 [Online]. Available: https://doi.org/10.1109/TAC.2011.2174666

[13] G. S. Seyboth, D. V. Dimarogonas, and K. H. Johansson, "Event-based broadcasting for multi-agent average consensus," *Automatica*, vol. 49, no. 1, pp. 245–252, 2013 [Online]. Available: https://doi.org/https://doi.org/10.1016/j.automatica.2012.08.042

[14] Y. Fan, L. Liu, G. Feng, and Y. Wang, "Self-triggered consensus for multi-agent systems with zeno-free triggers," *IEEE Transactions on Automatic Control*, vol. 60, no. 10, pp. 2779–2784, 2015 [Online]. Available: https://doi.org/10.1109/TAC.2015.2405294

[15] R. Yang, H. Zhang, G. Feng, H. Yan, and Z. Wang, "Robust cooperative output regulation of multi-agent systems via adaptive event-triggered control," *Automatica*, vol. 102, pp. 129–136, 2019 [Online]. Available: https://doi.org/https://doi.org/10.1016/j.automatica.2019.01.001

[16] W. Hu, L. Liu, and G. Feng, "Cooperative output regulation of linear multi-agent systems by intermittent communication: A unified framework of time- and event-triggering strategies," *IEEE Transactions on Automatic Control*, vol. 63, no. 2, pp. 548–555, 2018 [Online]. Available: https://doi.org/10.1109/TAC.2017.2727821

[17] Y.-Y. Qian, L. Liu, and G. Feng, "Output consensus of heterogeneous linear multi-agent systems with adaptive event-triggered control," *IEEE Transactions on Automatic Control*, vol. 64, no. 6, pp. 2606–2613, 2019 [Online]. Available: https://doi.org/10.1109/TAC.2018.2868997

[18] Z.-G. Wu, Y. Xu, R. Lu, Y. Wu, and T. Huang, "Event-triggered control for consensus of multiagent systems with fixed/switching topologies," *IEEE Transactions on Systems, Man, and Cybernetics: Systems*, vol. 48, no. 10, pp. 1736–1746, 2018 [Online]. Available: https://doi.org/10.1109/TSMC.2017.2744671

[19] B. Cheng, X. Wang, and Z. Li, "Event-triggered consensus of homogeneous and heterogeneous multiagent systems with jointly connected switching topologies," *IEEE Transactions on Cybernetics*, vol. 49, no. 12, pp. 4421–4430, 2019 [Online]. Available: https://doi.org/10.1109/TCYB.2018.2864974

[20] W. Hu, L. Liu, and G. Feng, "Event-triggered cooperative output regulation of linear multi-agent systems under jointly connected topologies," *IEEE Transactions on Automatic Control*, vol. 64, no. 3, pp. 1317–1322, 2019 [Online]. Available: https://doi.org/10.1109/TAC.2018.2849587

[21] Q. Jia and W. K. S. Tang, "Consensus of multi-agents with event-based nonlinear coupling over time-varying digraphs," *IEEE Transactions on Circuits and Systems II: Express Briefs*, vol. 65, no. 12, pp. 1969–1973, 2018 [Online]. Available: https://doi.org/10.1109/TCSII.2018.2790582

[22] Y. Han, W. Lu, and T. Chen, "Consensus analysis of networks with time-varying topology and event-triggered diffusions," *Neural Networks*, vol. 71, pp. 196–203, 2015 [Online]. Available: https://doi.org/https://doi.org/10.1016/j.neunet.2015.08.008

[23] Y. Hao, L. Liu, and G. Feng, "Event-triggered cooperative output regulation of heterogeneous multiagent systems under switching directed topologies," *IEEE Transactions on Cybernetics*, vol. 53, no. 2, pp. 1026–1038, 2023 [Online]. Available: https://doi.org/10.1109/TCYB.2021.3097337

[24] E. Xargay, "Time-critical cooperative path-following control of multiple unmanned aerial vehicles," Ph.D. dissertation, University of Illinois at Urbana-Champaign, 2013.

[25] H. K. Khalil, *Nonlinear Systems*. Prentice-Hall, Englewood Cliffs, NJ, 2002.

Initial Distribution List

Initial Distribution List

1. Defense Technical Information Center
   Ft. Belvoir, Virginia

2. Dudley Knox Library
   Naval Postgraduate School
   Monterey, California

3. Research Sponsored Programs Office, Code 41
   Naval Postgraduate School
   Monterey, CA 93943